4.4. Stability Analysis of the Core-Annular Flow.

To explain the observed phenomenon of formation of segregated structures the method of small perturbations and the linear stability analysis is applied. It is worth to remind that Tomotika [51] applied this method to explain the phenomenon of formation of drops observed by Taylor [50] - see chapter 2.5.

The stability of an axisymmetric core-annular flow shown schematically in figure 4.7 is considered. The core liquid has density and viscosity ρ_1 and μ_1 respectively; the annularly flowing liquid has properties ρ_2 and μ_2.

The equations of motion and continuity for both liquids (assumed to be incompressible, Newtonian and nondiffusive) have the following form:

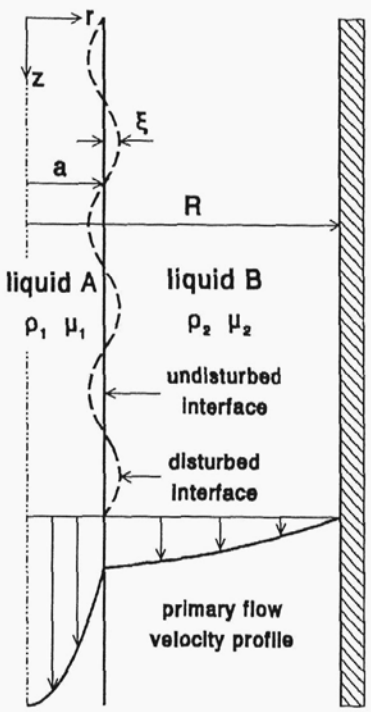

Figure 4.7. Sketch of the system.

$$\frac{\partial u}{\partial t}+u\cdot\frac{\partial u}{\partial r}+w\cdot\frac{\partial u}{\partial z}=-\frac{1}{\rho}\cdot\frac{\partial p}{\partial r}+\nu\cdot\left[\frac{\partial}{\partial r}\left(\frac{1}{r}\cdot\frac{\partial(r\cdot u)}{\partial r}\right)+\frac{\partial^2 u}{\partial z^2}\right], \tag{4.7a}$$

$$\frac{\partial w}{\partial t}+u\cdot\frac{\partial w}{\partial r}+w\cdot\frac{\partial w}{\partial z}=-\frac{1}{\rho}\cdot\frac{\partial p}{\partial z}+\nu\cdot\left[\frac{1}{r}\cdot\frac{\partial}{\partial r}\left(r\cdot\frac{\partial w}{\partial r}\right)+\frac{\partial^2 w}{\partial z^2}\right], \tag{4.7b}$$

$$\frac{1}{r}\cdot\frac{\partial(r\cdot u)}{\partial r}+\frac{\partial w}{\partial z}=0\ . \tag{4.8}$$

Assuming that the flow is axisymmetric and stationary one can reduce the system of equations (4.7) to the form:

$$U=0\ ,\qquad 0=-\frac{1}{\rho}\cdot\frac{\partial P}{\partial z}+\nu\cdot\frac{1}{r}\cdot\frac{\partial}{\partial r}\left(r\cdot\frac{\partial W}{\partial r}\right), \tag{4.9a}$$

which after integration with boundary and interfacial conditions:

$$W_1 \text{ finite at } r=0\ ,\quad W_1=W_2 \text{ and } \mu_1\cdot\frac{\partial W_1}{\partial r}=\mu_2\cdot\frac{\partial W_2}{\partial r} \text{ at } r=a\ ,\quad W_2=0 \text{ at } r=R \tag{4.9b}$$

gives the velocity distribution of the primary, core-annular flow:

$$W_1(r) = -\frac{1}{4}\cdot\frac{\partial P}{\partial z}\cdot\left(\frac{a^2-r^2}{\mu_1}+\frac{R^2-a^2}{\mu_2}\right) \qquad \text{for} \quad 0\le r\le a\ , \tag{4.10a}$$

$$W_2(r) = -\frac{1}{4}\cdot\frac{\partial P}{\partial z}\cdot\frac{R^2-r^2}{\mu_2} \qquad \text{for} \quad a\le r\le R\ . \tag{4.10b}$$

As it was explained in the literature review, the method of small perturbations assumes that velocities and pressure consist of their undisturbed values **(U, W, P)** and the small perturbations **(u′, w′, p′)**. Thus one has:

$$u = U + u'\ , \tag{4.11a}$$

$$w = W + w'\ , \tag{4.11b}$$

$$p = P + p'\ . \tag{4.11c}$$

The form of (4.11) is equivalent to the assumption that perturbations are axially symmetrical. Introducing now **u**, **w**, **p** from equations (4.11) into equations (4.7) and (4.8), neglecting the products of velocity and pressure perturbations (with themselves or with their derivatives) and taking into account the equations of unperturbed flow (4.9) results in:

$$\frac{\partial u'}{\partial t}+W\cdot\frac{\partial u'}{\partial z} = -\frac{1}{\rho}\cdot\frac{\partial p'}{\partial r}+\nu\cdot\left[\frac{\partial}{\partial r}\left(\frac{1}{r}\cdot\frac{\partial(r\cdot u')}{\partial r}\right)+\frac{\partial^2 u'}{\partial z^2}\right], \tag{4.12a}$$

$$\frac{\partial w'}{\partial t}+u'\cdot\frac{\partial W}{\partial r}+W\cdot\frac{\partial w'}{\partial z} = -\frac{1}{\rho}\cdot\frac{\partial p'}{\partial z}+\nu\cdot\left[\frac{1}{r}\cdot\frac{\partial}{\partial r}\left(r\cdot\frac{\partial w'}{\partial r}\right)+\frac{\partial^2 w'}{\partial z^2}\right], \tag{4.12b}$$

$$\frac{1}{r}\cdot\frac{\partial(r\cdot u')}{\partial r}+\frac{\partial w'}{\partial z}=0\ . \tag{4.13}$$

Following Tomotika [51], the velocity components of the perturbed flow can be expressed in terms of Stokes stream function:

$$u' = \frac{1}{r}\cdot\frac{\partial\psi}{\partial z}\ , \tag{4.14a}$$

$$w' = -\frac{1}{r}\cdot\frac{\partial\psi}{\partial r}\ . \tag{4.14b}$$

Elimination of pressure from equations of perturbed flow (4.12) and introduction of the stream function ψ reduces the system of equations (4.12) and (4.13) to the form:

$$\left(\frac{\partial}{\partial t}+W\cdot\frac{\partial}{\partial z}\right)\cdot D\psi-\frac{\partial\psi}{\partial z}\cdot r\cdot\frac{\partial}{\partial r}\cdot\left(\frac{1}{r}\cdot\frac{\partial W}{\partial r}\right)=\nu\cdot DD\psi\ , \tag{4.15}$$

where **D** is a differential operator

$$D\equiv\frac{\partial^2}{\partial r^2}-\frac{1}{r}\cdot\frac{\partial}{\partial r}+\frac{\partial^2}{\partial z^2}\ . \tag{4.16}$$

It should be noted, that equation of continuity (4.13) is automatically fulfilled by expressions (4.14).

Due to the axial symmetry of the flow one can expect [71] a solution of equation (4.15) in the following form:

$$\psi(r,z,t) = \phi(r) \cdot \exp[i \cdot \alpha (z - c \cdot t)] \ . \tag{4.17}$$

α and **c** are in equation (4.17) the wave number ($\alpha = 2 \cdot \pi / \lambda$) and the wave speed respectively. Introduction of ψ from equation (4.17) into equation (4.15) results in so-called Orr-Sommerfeld equation

$$(W-c) \cdot (L-\alpha^2) \cdot \phi(r) - \phi(r) \cdot r \cdot \frac{d}{dr}\left(\frac{1}{r} \cdot \frac{dW}{dr}\right) = \frac{\nu}{i \cdot \alpha} \cdot (L-\alpha^2)^2 \cdot \phi(r) \ , \tag{4.18}$$

where

$$L \equiv \frac{d^2}{dr^2} - \frac{1}{r} \cdot \frac{d}{dr} \ . \tag{4.19}$$

The system of differential equations (4.18) (first equation for the core liquid and the second one for the annular liquid) should be solved with the appropriate boundary and interfacial conditions. The first group of the boundary conditions requires the perturbation velocities to be finite at the coordinate axis:

$$u_1', \ w_1' \quad \text{finite at} \quad r = 0 \tag{4.20a}$$

and the second group sets the perturbation velocities to zero at the system border:

$$u_2' = w_2' = 0 \quad \text{at} \quad r = R \ . \tag{4.20b}$$

The conditions to be fulfilled on the liquid-liquid interface are:

- continuity of radial perturbation velocities

$$u_1' = u_2' \ , \tag{4.21a}$$

- bounding of the axial velocities

$$w_1' - w_2' + \left(\frac{dW_1}{dr} - \frac{dW_2}{dr}\right) \cdot \xi = 0 \ , \tag{4.21b}$$

- continuity of the tangential stress

$$\mu_1 \cdot \left(\frac{\partial u_1'}{\partial z} + \frac{\partial w_1'}{\partial r}\right) = \mu_2 \cdot \left(\frac{\partial u_2'}{\partial z} + \frac{\partial w_2'}{\partial r}\right) \ , \tag{4.21c}$$

- balance of the radial stress

$$\left(-p_1' + 2\cdot\mu_1\cdot\frac{\partial u_1'}{\partial r}\right) - \left(-p_2' + 2\cdot\mu_2\cdot\frac{\partial u_2'}{\partial r}\right) = \frac{\sigma}{a^2}\cdot\left(\xi + a^2\cdot\frac{\partial^2\xi}{\partial z^2}\right) . \qquad \textbf{(4.21d)}$$

In the above expressions symbol ξ denotes the displacement of the interface from its initial position in the radial direction as shown in figure 4.7. The disturbance of the interface - ξ is related to the radial perturbation velocity by:

$$u_1'(a) = W_1(a)\cdot\frac{\partial\xi}{\partial z} + \frac{\partial\xi}{\partial t} . \qquad \textbf{(4.22)}$$

Using now equations (4.14a) and (4.17) to eliminate $\mathbf{u_1'}$ from equation (4.22) one receives:

$$\xi(z,t) = \frac{\phi_1(a)}{a\cdot\left(W_1(a) - c\right)}\cdot\exp[i\cdot\alpha\cdot(z - c\cdot t)] . \qquad \textbf{(4.23)}$$

This allows to conclude that at the initial stages of destabilization the disturbance of the liquid-liquid interface can be interpreted as a superposition of sinusoidal waves.

The boundary conditions (4.21b) and (4.21d) result in destabilization of the flow due to discontinuity of velocity gradient in the primary flow ($\mu_1 \neq \mu_2$) or discontinuity of the normal stress (σ**>0**). In the considered case the liquids are completely miscible, so σ **= 0**. Introduction of equations (4.14) and (4.17) into the boundary and interfacial conditions yields:

- at r=0 $\quad \frac{\phi_1}{r}$, $\frac{1}{r}\cdot\frac{d\phi_1}{dr}$ finite , **(4.24a)**

- at $r = R$ $\quad \phi_2 = \frac{d\phi_2}{dr} = 0$ **(4.24b)**

and at **r=a**:

$$\phi_1 = \phi_2 , \qquad \textbf{(4.25a)}$$

$$(c - W_1)\cdot\left(\frac{d\phi_1}{dr} - \frac{d\phi_2}{dr}\right) + \left(\frac{dW_1}{dr} - \frac{dW_2}{dr}\right)\cdot\phi_1 = 0 , \qquad \textbf{(4.25b)}$$

$$\mu_1\cdot\left(L + \alpha^2\right)\cdot\phi_1 = \mu_2\cdot\left(L + \alpha^2\right)\cdot\phi_2 , \qquad \textbf{(4.25c)}$$

$$\begin{aligned}&\frac{\mu_1}{i\cdot\alpha\cdot a}\cdot\frac{d}{dr}\left(L - \alpha^2\right)\cdot\phi_1 + 2\cdot i\cdot\alpha\cdot\mu_1\cdot\frac{d}{dr}\left(\frac{\phi_1}{r}\right) + \frac{\rho_1\cdot\phi_1}{a}\cdot\frac{dW_1}{dr} + \frac{\rho_1\cdot(c - W_1)}{a}\cdot\frac{d\phi_1}{dr} + \\ &- \frac{\mu_2}{i\cdot\alpha\cdot a}\cdot\frac{d}{dr}\left(L - \alpha^2\right)\cdot\phi_2 - 2\cdot i\cdot\alpha\cdot\mu_2\cdot\frac{d}{dr}\left(\frac{\phi_2}{r}\right) - \frac{\rho_2\cdot\phi_2}{a}\cdot\frac{dW_2}{dr} - \frac{\rho_2\cdot(c - W_2)}{a}\cdot\frac{d\phi_2}{dr} = 0 .\end{aligned} \qquad \textbf{(4.25d)}$$

Obviously, the Orr-Sommerfeld equations (4.18) and the stated above boundary and interfacial conditions are satisfied by $\phi_1 \equiv \phi_2 \equiv 0$. On the other hand, only a discrete spectrum of the axisymmetric disturbances exists if ϕ_1 and ϕ_2 are not equal to zero in the whole flow domain [71]. The amplitude of these perturbations should grow or decrease with time, depending on the sign of the imaginary part of the wave speed - **Im(c)**. When **Im(c)>0** then the amplitude of corresponding disturbance increases exponentially, when **Im(c)<0** then the amplitude decreases exponentially. In the case, when **Im(c)=0** the perturbation will neither grow nor diminish.

Assuming that the fastest growing disturbance becomes the dominant, one can expect forming initially periodic structures due to local periodic thinning and thickening of the central thread. The distance between the narrowings is related to the wavelength of the fastest growing disturbances. In a single phase system the periodic segregated structures should be persistent. In the two-phase system the interfacial surface tension finally disrupts the destabilized central stream in narrowings into separate drops what is generally observed in practice.

The relation between the wave number - α and the rate of growth of the wave amplitude - $\alpha \cdot$**Im(c)** is given by the system of two Orr-Sommerfeld equations (4.18) with boundary (4.24) and interfacial conditions (4.25). Using equations (4.10) for the primary flow the Orr-Sommerfeld equations are reduced to the form:

$$(W_i - c)\cdot(L-\alpha^2)\cdot\phi_i(r) = \frac{\nu_i}{i\cdot\alpha}\cdot(L-\alpha^2)^2\cdot\phi_i(r) \qquad \text{for } i=1,2\ . \tag{4.26}$$

The solution of equation (4.26) can be now approximated by the finite series of the modified Chebyshev polynomials:

$$\phi_1(x) = \frac{a_0}{2}\cdot T_0^*(x) + a_1\cdot T_1^*(x) + a_2\cdot T_2^*(x) + ... + a_k\cdot T_k^*(x) \quad \text{where } x = \frac{r}{a}\ , \tag{4.27a}$$

$$\phi_2(y) = \frac{b_0}{2}\cdot T_0^*(y) + b_1\cdot T_1^*(y) + b_2\cdot T_2^*(y) + ... + b_l\cdot T_l^*(y) \quad \text{where } y = \frac{r-a}{R-a}\ , \tag{4.27b}$$

which transforms equations (4.24), (4.25) and (4.26) into the system of algebraic equations. The "tau" method was applied to the resulting system of algebraic equations and a general eigenvalue problem was formulated (for details and references see appendix C):

$$\overline{\overline{A}}\cdot\bar{v} = c\cdot\overline{\overline{B}}\cdot\bar{v}\ , \tag{4.28}$$

where $\overline{\overline{\mathbf{A}}}$ and $\overline{\overline{\mathbf{B}}}$ represent system matrices and symbol $\bar{\mathbf{v}}$ denotes the vector of the coefficients

$[a_0,a_1,a_2,...,a_k,b_0,b_1,b_2,...,b_l]$. The eigenvalues of (4.28) were computed by means of the LZ-algorithm.

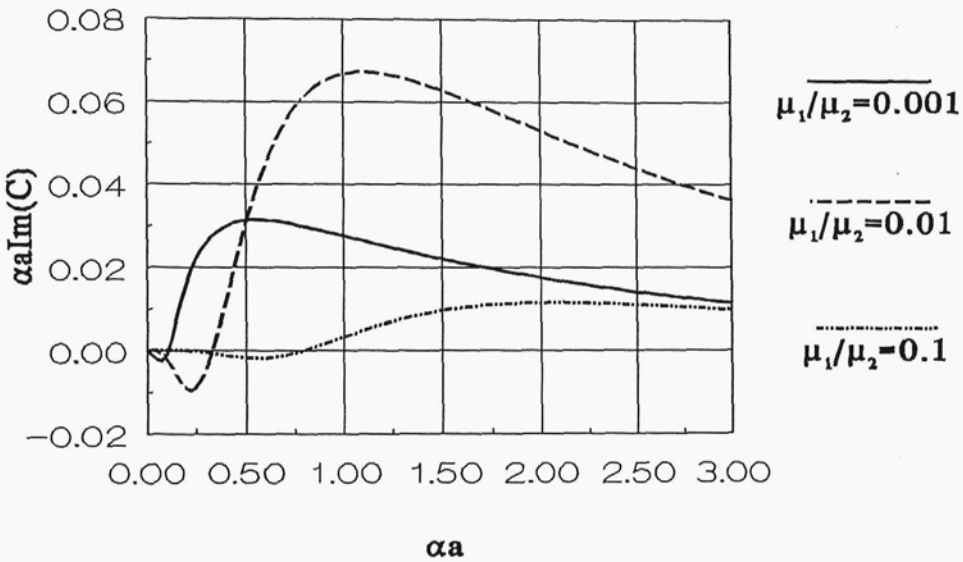

Figure 4.8. Effect of viscosity ratio on stability of the core-annular flow; $\rho_1/\rho_2 = 1$, $a / R = 0.1$, $W_1(0)\cdot a\cdot\rho_1/\mu_1 = 10$.

Figure 4.8 shows results of calculations obtained for the case when less viscous liquid flows in the core. Analysis of this figure shows that decreasing the viscosity ratio μ_1/μ_2 shifts the wave number of the fastest growing disturbances to lower values and consequently increases its wavelength. The influence of the viscosity ratio μ_1/μ_2 on dimensionless frequency

$$\alpha \cdot a \cdot Im(C) = \alpha \cdot a \cdot \frac{Im(c) \cdot a \cdot \rho_1}{\mu_1} \qquad (4.29)$$

seems to be more complicated because one can observe a maximum of $\alpha\cdot a\cdot Im(C)$ appearing for the intermediate viscosity ratio. It seems that the perturbing action of the discontinuous velocity gradient may be changed by the high viscosity of liquid located annularly. The range of unstable waves extends far behind $\alpha\cdot a=1$, whereas the longest waves ($\alpha\cdot a \to 0$) may become stable. This interval of stability was predicted by Hickox [55] in his analysis performed for very long waves and as it can be seen this interval extends with the increasing viscosity ratio.

The influence of the radius of the core in the primary flow on the stability curve is presented in figure 4.9. For low value of ratio **a/R** increasing the core radius increases the rate of growth of perturbation without much influence on the position of the fastest growing disturbance.

Let us compare the theory with the experimental results. For this purpose, it has been assumed that the average distance between successive narrowings of the core stream is equal to the

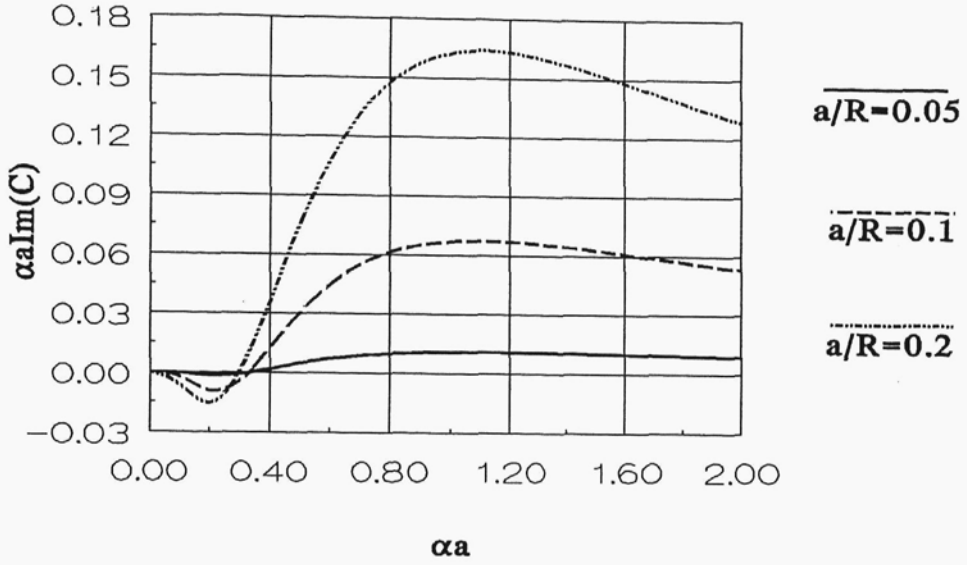

Figure 4.9. Effect of interface position on the stability of the core-annular flow; $\rho_1/\rho_2 = 1$, $\mu_1/\mu_2 = 0.01$, $W_1(0)\cdot a\cdot\rho_1/\mu_1 = 10$.

wavelength of a disturbance. This distance was measured on photographs. The measurements were performed on the structures in the cylindrical section of the mixer. The radius of the undisturbed liquid-liquid interface was calculated from:

$$a = R\cdot\sqrt{Q_1}\Big/\sqrt{Q_2+Q_1+\sqrt{Q_2\cdot(Q_2+Q_1\cdot\mu_2/\mu_1)}}\ , \tag{4.30}$$

whereas the maximum velocity of the primary flow and related to it Reynolds number from:

$$W_1(0) = \frac{Q_1}{\pi\cdot a^2}\cdot\left(\frac{a^2}{\mu_1}+\frac{R^2-a^2}{\mu_2}\right)\Big/\left(\frac{a^2}{2\cdot\mu_1}+\frac{R^2-a^2}{\mu_2}\right), \tag{4.31}$$

$$Re_w = W_1(0)\cdot a\cdot\rho_1/\mu_1\ . \tag{4.32}$$

Equations (4.30) and (4.31) follow directly from the velocity profiles described by equations (4.10). Table 4.VII shows values of dimensionless wave numbers obtained in the experiments. Stability curves computed from the same experimental conditions are shown in figure 4.10. The theoretical $\alpha\cdot a$ values corresponding to the maximum instability are close to 0.7, whereas the observed values of $\alpha\cdot a$ are close to 1. The fastest

Table 4.VII. Experimental results.

Exp.No.	a[mm]	λ[mm]	Re_w	$\alpha\cdot a$
5	1.046	6.7	5.68	0.981
6	1.353	8.4	9.87	1.012
7	1.761	10.7	18.6	1.034
8	2.102	10.5	29.8	1.258
9	2.665	-	65.8	-

growth of the disturbances is predicted for large flow rates of the less viscous fluids, which agrees with the photographs of the flow. The agreement is fairly satisfactory; one should remember at this point that the idea that the fastest growing disturbance may become the dominant one "is not necessarily correct in view of initial conditions and of nonlinearity but is often a good working rule" [71, p.25]. One can also see on the photographs that the wavelength close to the feeding pipe is usually longer than the average one; this value is, however, difficult to measure precisely, so it was not used for comparison.

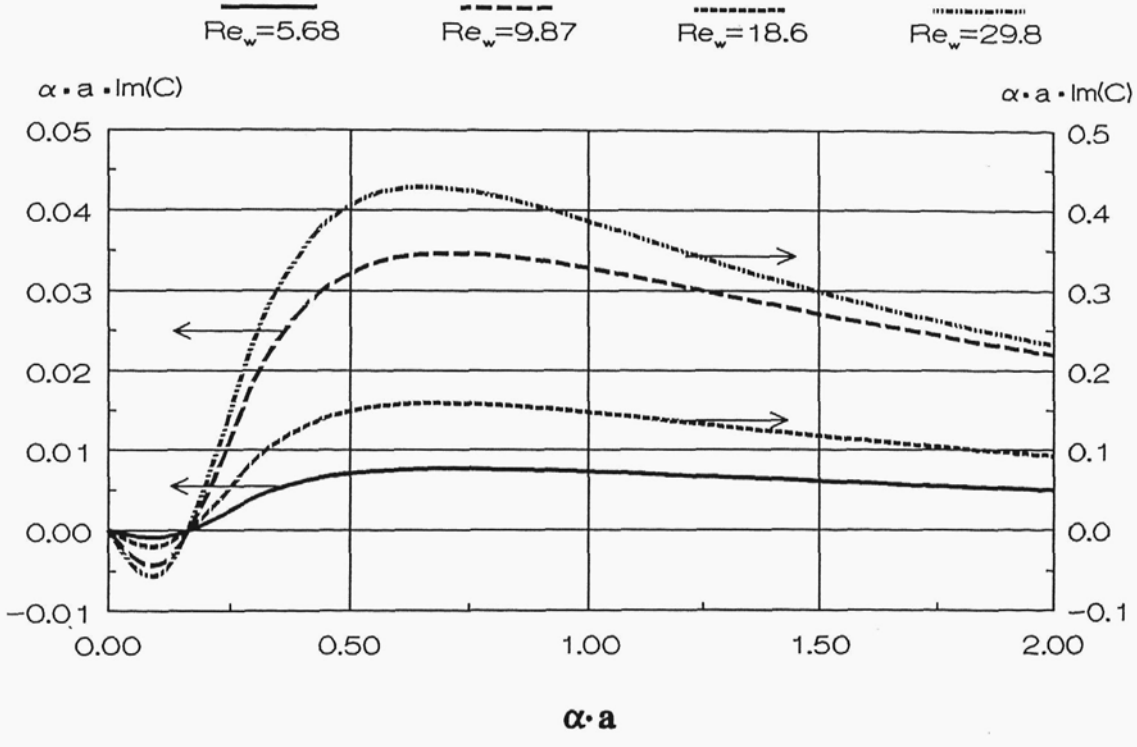

Figure 4.10. Stability curves obtained for experimental conditions; exp.no. 5÷8.

Although it is always possible to perform a complete analysis of stability of simple flows, it would be useful to formulate some rules determining the flow behavior. Some of these rules were formulated in the literature [55,56]. The present study confirmed some of these observations but also revealed other interesting features of the core-annular flow in the case when the liquids are completely miscible. Numerical computations performed for viscosity ratio μ_1/μ_2 ranging from 0.001 to 0.1 (less viscous liquid in core) and for small core radiuses ($0.025 \le a/R \le 0.2$) allowed to formulate the following conclusions.

Firstly, it was found that the influence of Reynolds number, $\mathbf{Re_w}$, on the appearance of instabilities and their wavelength is very limited. Figures 4.11ab show curves dividing the whole spectrum of wave numbers on the regions of stable, long waves (below the curve) and unstable short waves (above the curve).

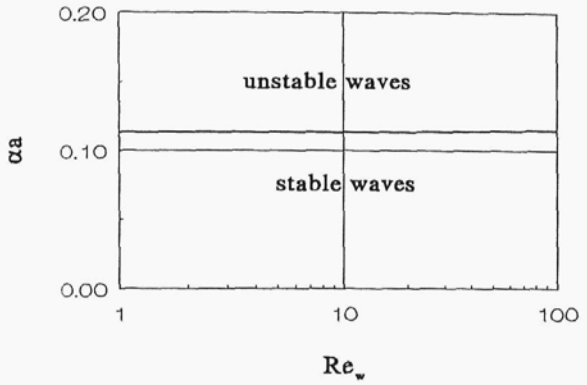

Figure 4.11a. μ_1/μ_2**=0.001,** **a/R=0.05,** ρ_1/ρ_2**=1.**

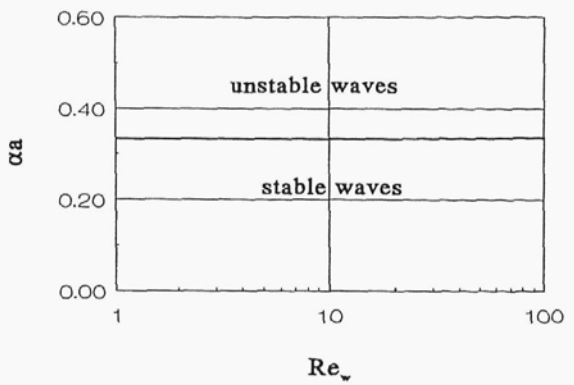

Figure 4.11b. μ_1/μ_2**=0.01** **a/R=0.05,** ρ_1/ρ_2**=1.**

Stability of axisymmetric disturbances.

Increasing Reynolds number from 1 to 100 has a very small effect on the width of the stability region. As Reynolds number grows the region of stability slightly increases in the direction of short waves (higher values of $\alpha \cdot a$). The sensitivity to $\mathbf{Re_w}$ increases with the increase of the viscosity ratio μ_1/μ_2. In the situation shown in figure 4.11c, obtained for μ_1/μ_2**=0.1**, stable are disturbances of intermediate wavelengths. Both very long waves and short waves are unstable. It can be shown that for μ_1/μ_2**=0.1**, increasing Reynolds number shifts the region of stability to the smaller wave numbers. The upper limit of stability is only slightly decreased, while the lower limit decreases by 45% when Reynolds number grows from 1 to 100. The results presented in figures 4.11abc can be safely extended for Reynolds numbers lower than one, where the curves representing neutral disturbances (neither growing or diminishing) become flat.

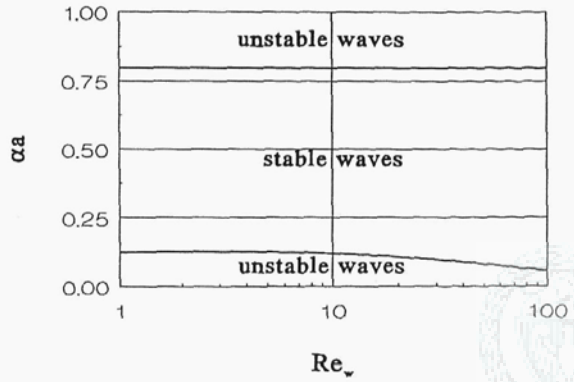

Figure 4.11c. Stability of axisymmetric disturbances; μ_1/μ_2**=0.1, a/R=0.05,** ρ_1/ρ_2**=1.**

Obviously, the knowledge of the location and width of the stability region is insufficient to predict appearance of axisymmetric disturbances. However, it allows to exclude from the whole spectrum of wave numbers the disturbances that cannot grow.

Secondly, the computations performed for different values of the ratio **a/R** confirm the results shown in figures 4.11abc. The general rule is such that the influence of the ratio **a/R** on the region of stability depends on the value of μ_1/μ_2. When the ratio μ_1/μ_2 is small decreasing the radius of the core stream flattens the curves of neutral disturbances, whereas increasing this

radius reduces the region of stability. This region vanishes for **a/R** higher than a critical value - see figure 4.12a. For higher values of μ_1/μ_2, either decreasing or increasing of the ratio **a/R** can extended the region of stability, as shown in figure 4.12b.

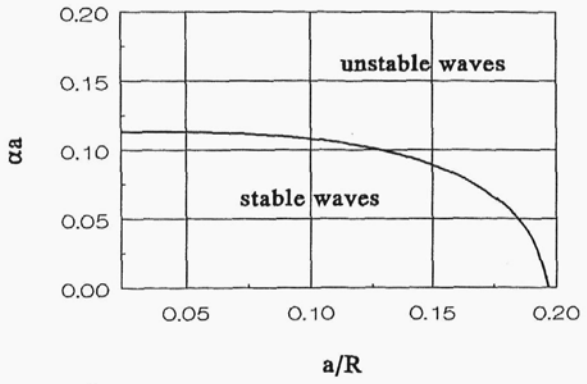

Figure 4.12a. μ_1/μ_2**=0.001,** Re_w**=1,** ρ_1/ρ_2**=1.**

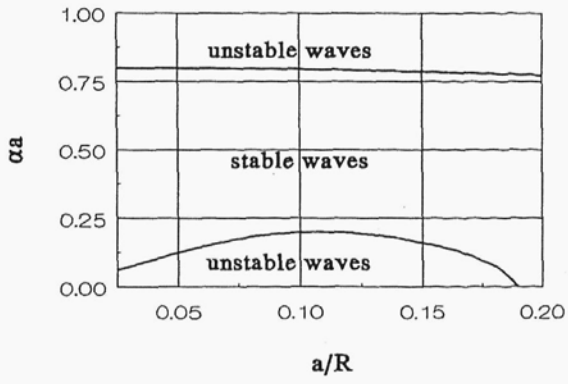

Figure 4.12b. μ_1/μ_2**=0.1** Re_w**=1,** ρ_1/ρ_2**=1.**

Stability of axisymmetric disturbances.

One can conclude, that if there is considerable variation of viscosity in mixed liquids, it can result in instabilities of deforming flows and the process of mechanical thinning can be retarded by formation of periodic, segregated structures. The present study provides both the experimental proof of this hypothesis and its theoretical confirmation. The considered phenomenon was found to be very complex and difficult to predict in advance. One should, however, have this possibility in mind when using lamellar structures models [22,23] for mixing of liquids differing widely in viscosity.